# An optical authentication system based on imaging of excitation-selected lanthanide luminescence

Carro-Temboury, Miguel R.; Arppe, Riikka Matleena; Vosch, Tom André Jos; Sørensen, Thomas Just

*Published in:*
Science Advances

*DOI:*
10.1126/sciadv.1701384

*Publication date:*
2018

*Document version*
Publisher's PDF, also known as Version of record

APPLIED SCIENCES AND ENGINEERING

# An optical authentication system based on imaging of excitation-selected lanthanide luminescence

Miguel R. Carro-Temboury,* Riikka Arppe,* Tom Vosch,† Thomas Just Sørensen†



**Secure data encryption relies heavily on one-way functions, and copy protection relies on features that are difficult to reproduce. We present an optical authentication system based on lanthanide luminescence from physical one-way functions or physical unclonable functions (PUFs). They cannot be reproduced and thus enable unbreakable encryption. Further, PUFs will prevent counterfeiting if tags with unique PUFs are grafted onto products. We have developed an authentication system that comprises a hardware reader, image analysis, and authentication software and physical keys that we demonstrate as an anticounterfeiting system. The physical keys are PUFs made from random patterns of taggants in polymer films on glass that can be imaged following selected excitation of particular lanthanide(III) ions doped into the individual taggants. This form of excitation-selected imaging ensures that by using at least two lanthanide(III) ion dopants, the random patterns cannot be copied, because the excitation selection will fail when using any other emitter. With the developed reader and software, the random patterns are read and digitized, which allows a digital pattern to be stored. This digital pattern or digital key can be used to authenticate the physical key in anticounterfeiting or to encrypt any message. The PUF key was produced with a staggering nominal encoding capacity of $7^{3600}$. Although the encoding capacity of the realized authentication system reduces to $6 \times 10^{104}$, it is more than sufficient to completely preclude counterfeiting of products.**

## INTRODUCTION

Secure communication and authentication of products pose major societal challenges. An optical authentication system based on physical unclonable functions (PUFs) may provide the solution. Using PUFs in an anticounterfeiting system will address the billion-dollar economic losses imposed by counterfeiting (*1*–*3*) and can potentially save lives if used to guarantee the authenticity of medicine (*4*–*8*). The randomness inherent in PUFs can be used for unbreakable public key encryption (*9*). The decryption key cannot be guessed, and because a PUF, by definition, cannot be copied, only the key holder may decipher the encrypted message. Here, we present a new optical authentication system based on PUF patterns of lanthanide-doped zeolite taggants in polymer films that are read using excitation-selected imaging of the lanthanide dopants. The system is demonstrated in the context of an anticounterfeiting system.

In anticounterfeiting, the established technologies all use tags that are the result of a deterministic process (*10*, *11*). As a consequence, they all rely on restricted access to the ink or printing technology, which makes them susceptible to counterfeiting—even DNA tags are readily read and copied if a suitable incentive is present (*10*, *12*). The highly secure encoding method presented here is different in nature because it uses statistically unique physical keys based on PUFs (*13*), which are based on nondeterministic, random features of the anticounterfeiting tag, making it impossible to duplicate even by the manufacturer, let alone the counterfeiters (*13*–*21*).

The presented authentication system is based on physical keys made from physical one-way functions better known as PUFs (*14*, *22*–*24*). We make these unique random patterns in a stochastic process, where taggants supported in a polymer thin film create a random pattern on the substrate of choice (*16*). By imaging a selected area of the thin film, a unique physical key is created. Such a PUF key can be tagged onto every single blister pack of pills or designer hand bag, and each product will feature a unique key. All physical keys are read, and their digital keys are stored in a database, thereby allowing each product to be uniquely identified throughout the supply chain.

The physical key is read using three, energetically closely spaced, blue laser lines, each selectively exciting different lanthanide ions. The emission following the selective excitation is used to image the key. The control of excitation light rather than emission light resolves the different taggants used to form the unique pattern that is the PUF key. Upon each excitation wavelength, a different and unique random pattern emerges, and the digitized and combined pattern forms the unique digital key. This new method of reading the random pattern is different from known methods of optical multiplexing, which are read by analyzing the color composition of the emitted light (*12*, *25*). When this new readout mode is combined with unique parameters for digitizing and comparing readouts, we have created a tamper-proof optical authentication system.

Here, we demonstrate the excitation-resolved optical authentication concept for anticounterfeiting using physical keys made from zeolites doped with europium(III), terbium(III), or dysprosium(III) ions immobilized in a polyvinyl alcohol (PVA) thin film (see Fig. 1). We exploit the narrow absorption lines of the lanthanides and lanthanide centered emission to resolve up to three binary responses, depending on the presence or absence of a given lanthanide in a given pixel (see Fig. 1). By using three lanthanide(III) ions, we achieve very high encoding capacities. The encoding capacity of our system ($c^p$) is defined by the number of possible responses exhibited by a random pattern (see Fig. 1). With three lanthanide(III) ions, we can achieve seven different responses, which we visualize using a standard color scheme ($c = 7$; RGB-CMYK). In the examples presented here, we image an area of 60 pixels × 60 pixels ($p = 3600$), which gives a maximal encoding capacity of the proposed authentication system of $7^{3600}$. Because the encoding capacity of the random pattern is infinite for all practical purposes, there will never be two identical keys, ensuring that the physical keys are impossible to copy.

Multiplexing with a matrix of graphical or optical codes is a known concept for anticounterfeiting, tracking, and authentication purposes

Nano-Science Center and Department of Chemistry, University of Copenhagen, Universitetsparken 5, 2100 København Ø, Denmark.
*These authors contributed equally to this work.
†Corresponding author. Email: tom@chem.ku.dk (T.V.); TJS@chem.ku.dk (T.J.S.)

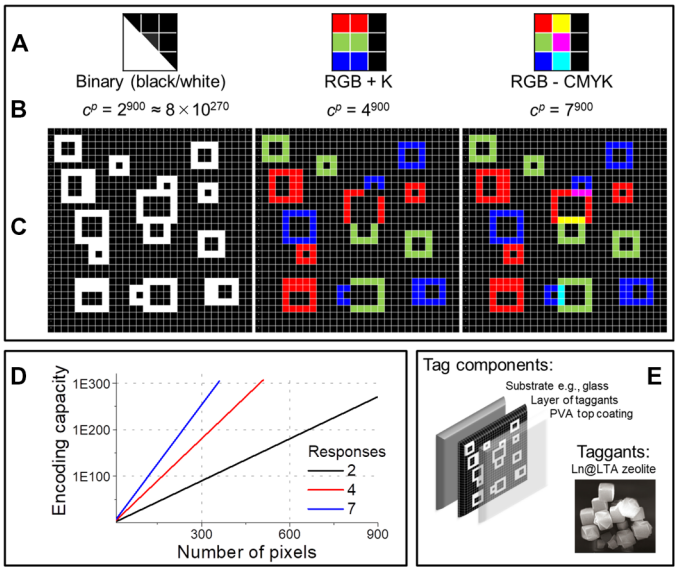


**Fig. 1. PUFs made from lanthanide(III)-doped zeolites in polymer thin films.** PUFs are random patterns, made from three different optically active taggants immobilized in a polymer thin film on a substrate and imaged using 30 pixels × 30 pixels. (**A**) The pattern can be read by resolving two, four, or seven optical responses. (**B**) The maximum encoding capacity of the pattern scales with the number of possible responses and the number of pixels read. (**C**) A cartoon representation of the same pattern read using two (binary), four (RGB+K), and seven (RGB-CMYK) responses. (**D**) Maximum encoding capacity as a function of the number of pixels used. (**E**) A random pattern made in a stochastic process by casting a solution of lanthanide-doped LTA zeolites and a polymer matrix onto a glass substrate (zeolite image from http://eng.thesaurus.rusnano.com/wiki/article1965).

(*26*, *27*). Optical multiplexing has been achieved by incorporating multiple organic dyes (*28*) or quantum dots (*29*–*31*) in different ratios into microspheres. The encoding capacity of the microspheres with fluorescent dyes is limited to ~$10^2$, whereas with quantum dots, it can be theoretically increased to $10^6$. However, the real encoding capacity is compromised by the broad and overlapping emission peaks, interference from background luminescence, and by variations in the anticounterfeiting tags with time due to photobleaching (*32*). By using lanthanide centered emission, we eliminate all these issues and significantly increase the encoding capacity. We can use lanthanide luminescence due to recent advances in laser and detector technology. Lanthanide-based dyes are highly photostable and absorb and emit light in well-defined regions of the electromagnetic spectrum (*33*). The narrow absorption and emission bands originate from electronic transitions within the shielded 4*f* shell and are observed across the visible spectrum in a barcode-like pattern that is unique to a given lanthanide (*33*), and the emission signatures are easily separated from emission from other sources and readily assigned to a specific lanthanide (*34*, *35*). The issue with using lanthanide(III) ions directly is that electronic transitions have small absorption cross sections, but state-of-the-art technology negates this problem. Their weak light absorptivity has also been circumvented by the antenna effect of molecular ligands (*33*, *36*) or by incorporating a large number of the lanthanide ions into an inorganic crystal (*33*, *37*). We use a high density of lanthanide(III) ions doped in a zeolite crystal. The lanthanide(III) ion cannot bleach, and the highly robust zeolite host ensures that the physical keys will not change in time.

## RESULTS AND DISCUSSION

An anticounterfeiting or authentication system based on PUFs consists of several elements. First, there is the physical key—here, a physical random pattern or PUF key—that is read using a specific hardware. The readout—here, an image—is digitized using a specific set of parameters creating the digital key, which is stored in a database. For anticounterfeiting, the process is performed at the point of origin of the product, and subsequent authentication then relies on rereading the physical key and converting the readout to a new digital key. This new digital key is then authenticated by comparing it to the stored digital key using dedicated software.

### The physical key

We made the physical key by producing a random pattern formed from taggants made from zeolite 5A [Linde Type A (LTA)], where the counterions ($Ca^{2+}$) have been exchanged by the relevant lanthanide(III) ions (see the Supplementary Materials for details) (*38*). The taggants are thus zeolites (microporous crystalline aluminosilicates) exchanged using an aqueous solutions of europium(III), terbium(III), and dysprosium(III) cations. The zeolites used are cubes with 2- to 4-μm edges (Fig. 1E). The three different taggants (Eu@LTA, Tb@LTA, and Dy@LTA) were mixed in water containing 3% (w/v) PVA [molecular weight ($M_w$) = 13,000 to 23,000], and the resulting suspension was spin-coated onto a microscope glass slide to form the random patterns with the properties represented in cartoon form in Fig. 1. The random patterns can be embossed in steel or leather, or the doped zeolites can be encased in glass. The stability of the random pattern and, thus, the physical key is determined by the substrate material used. Here, PVA on glass was used, where PVA is the limiting material. PVA is stable up to 200°C but is water-soluble. We did not observe any issues with stability of the physical keys over 18 months at ambient conditions but realize that a glass support may be too fragile and that water-soluble glue is not ideal for real-world applications. A selection of other tags on paper and glass are shown in the Supplementary Materials.

### The readout

When the zeolites are doped with lanthanide ions, the narrow absorption and emission bands resulting from lanthanide centered emission can both be used to resolve the optical response (Fig. 2). Emission-resolved imaging allows the three taggants to be differentiated using their unique emission spectra (Fig. 2A), whereas the excitation-resolved imaging differentiates them on the basis of unique absorption bands (Fig. 2B). In the latter case, the emission can be recorded from the lanthanide-loaded zeolites following excitation using a wavelength that addresses an absorption band of the targeted lanthanide ion (Fig. 2B); each of the selected lanthanide ions—$Eu^{3+}$, $Tb^{3+}$, and $Dy^{3+}$—may be addressed individually (Fig. 2B), which allows the emission of each lanthanide ion to be resolved despite overlapping emission spectra (Fig. 2A). The two methods have very different requirements when designing hardware for optical authentication of the random patterns: Emission-resolved method requires either a spectrometer or a filter-based detection, whereas for excitation-resolved method, only a single long-pass filter and a total intensity detector are enough to collect the emission, because only one lanthanide emits upon one selected excitation line. Further, if a filter-based hardware unit is used for emission-resolved readout, then it may be emulated using other emitters, whereas the excitation-resolved readout cannot because no other emitters have the narrow absorption bands exhibited by the lanthanide(III) ions. Thus, the excitation-selected readout adds an additional layer of security to the physical key.

Whereas emission-resolved imaging is well established, excitation-resolved imaging using close-lying absorption bands is not. To demonstrate that we are achieving excitation-resolved images, we used physical keys made using single taggants (Eu@LTA, Tb@LTA, or Dy@LTA). The taggants can be imaged following excitation at 450 nm for dysprosium, 465 nm for europium, and 488 nm for terbium. The images and spectra in Fig. 3 were recorded using a charge-coupled device (CCD)–based spectrometer (*39*, *40*), and the emission spectra were recorded for each pixel. The narrow barcode-like emission lines leave no doubt as to the nature of the emitting species. The dysprosium emission is significantly weaker than that of europium or terbium but still detectable. The weaker signal of $Dy^{3+}$ is predictable and due to nonradiative deactivation by high-energy O–H oscillators of water molecules trapped in the zeolite (*33*).

To further validate the excitation-selected imaging, we imaged the same physical key containing all three Ln taggants using spectrally resolved imaging (CCD-based spectrometer as detector) and excitation-resolved imaging [avalanche photodiode (APD) detector with a 532-nm long-pass filter]. The result is shown in Fig. 4, where the thin film was imaged using 465-, 488-, and 450-nm excitation wavelengths individually or all simultaneously. The emission spectra of each pixel were recorded and used to verify the origin of the recorded photons following excitation at the selected wavelength (see fig. S9). Cursory inspection of Fig. 4 shows that excitation-resolved imaging using lanthanide centered emission is as effective a tool as spectrally resolved imaging, demonstrating that either method outlined in Fig. 2 may be used to resolve the binary response of a random pattern formed by these taggants (see the Supplementary Materials for details). The images in Fig. 4 show that the dysprosium centered emission is very weak when compared to the terbium and europium centered emissions; too weak to perform well in fluorescence microscopy but sufficient to be used in excitation-selected multiplexing (see below).

More than one lanthanide has to be used in the PUF key because the method relies on the fact that the image cannot be emulated by other means. The narrow energy range used for excitation is deliberate, because all other emitters would be excited by all three excitation lines. Thus, an anticounterfeiting tag cannot be copied by bleaching of organic dyes or clever positioning of quantum dots, because these will emit in all channels. The lanthanide ions used here give very good contrast in excitation-selected imaging, particularly the combination using only europium and terbium. Micromanipulation of doped zeolites is theoretically possible, but the time and equipment needed to copy a single key combined with frequent validation eliminate the risk posed from such a laborious endeavor.

To obtain our readout, we used a homebuilt microscope. The next step in developing the optical authentication system will be to manufacture dedicated readers that can be placed throughout the supply chain. The reader hardware must be of a quality that ensures that the readout is within the specifications required by the digitization procedures for each individual reader and thus between the points in the supply chain. The digitization tolerates a specific error in each channel of the readout (see below and the Supplementary Materials). Different reader hardware will result in different readouts. Thus, a change of reader hardware changes the entire authentication system.

## The digital key

By increasing the number of possible responses in each pixel, excitation selection gives a higher spatial density encoding capacity than scattering-based methods, thus removing a possible limitation imposed by a low

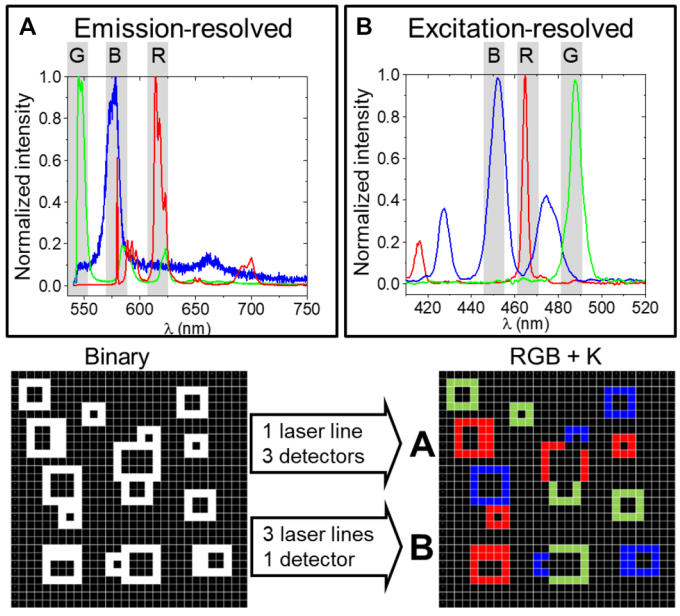


**Fig. 2. Light emission and absorption are equal when it comes to resolving random patterns of lanthanide(III)-doped zeolites.** (**A** and **B**) The emission (A) and the excitation (B) spectra resulting from lanthanide centered emission from zeolites doped with $Eu^{3+}$ (red), $Tb^{3+}$ (green), and $Dy^{3+}$ (blue) ions. Both emission and excitation information can be used to resolve the binary optical response (taggant is absent or present in a pixel) from a random pattern of doped zeolites in a polymer film into four channels (RGB+K).

encoding capacity of the resulting authentication systems (*16*). The multiple responses add complexity in the digital key because reading the physical key requires that three images are recorded using three different, energetically closely spaced, excitation wavelengths. Here, 465-, 488-, and 450-nm laser lines were used. The total intensity of each pixel is then recorded for each excitation channel and digitized in a binary form. The three images are then combined, where a color is designated for pixels where emission is detected following excitation using a specific laser line. We assigned letters/colors to pixels where emission is detected following excitation by a specific laser line: R to 465 nm ($Eu^{3+}$), G to 488 nm ($Tb^{3+}$), and B to 450 nm ($Dy^{3+}$). Thus, the three digitized images can be combined into one RGB digital key where the absence of a signal corresponds to black (R = 0, G = 0, and B = 0 [000]), whereas a signal in only one of the channels gives rise to the primary RGB colors (red [100], green [010], and blue [001]). Because the encoding capacity is defined by the number of pixels imaged ($p$) and the number of possible responses, this digital key has an encoding capacity of $4^p$ (see the Supplementary Materials for details). By including colocalization in the digitization procedure, the number of responses can be increased to seven with an encoding capacity of $7^p$. This can be achieved by decreasing the resolution in the image so that more than one taggant is present in each pixel or by including more than one lanthanide(III) ion in each taggant. When including colocalization, the colors are still defined by the number of excitation wavelengths that give rise to a signal, but now, signals in more than one channel are included as additional colors: yellow [110], magenta [101], and cyan [011]. White [111], with emission detected in all three channels, will not occur because of the noise reduction protocol used in the digitization procedure (see the Supplementary Materials). If the resolution or

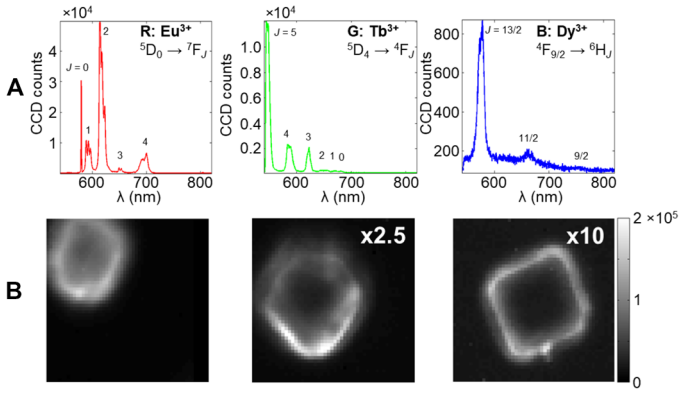


**Fig. 3. Emission-resolved images of zeolites doped with europium(III), terbium(III), and dysprosium(III) ions.** (**A**) Emission spectra of $Eu^{3+}$-, $Tb^{3+}$-, and $Dy^{3+}$-doped zeolites recorded upon 465-, 488-, or 450-nm excitation, respectively, from a single pixel with the CCD-based spectrometer system using 6.4- to 7.2-μW excitation power and 20-s integration time. (**B**) The corresponding confocal fluorescence image of $Eu^{3+}$-, $Tb^{3+}$-, and $Dy^{3+}$-doped zeolites (10 μm × 10 μm, 50 pixels × 50 pixels, and 1- to 2-s integration time). Intensities in $Tb^{3+}$ and $Dy^{3+}$ images are multiplied by the factor indicated.

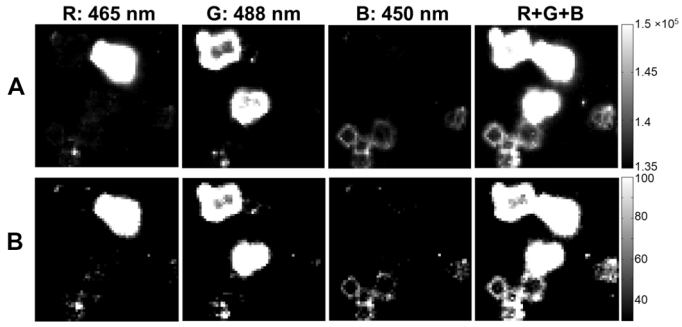


**Fig. 4. Comparing emission- and excitation-resolved images of zeolites doped with europium(III), terbium(III), and dysprosium(III) ions.** The three excitation wavelengths (R, 465 nm; G, 488 nm; and B, 450 nm) were first used separately and then simultaneously (R + G + B) to identify each taggant. (**A**) Emission-resolved images of a mixture of $Eu^{3+}$-, $Tb^{3+}$-, and $Dy^{3+}$-doped zeolites (30 μm × 30 μm, 60 pixels × 60 pixels, 1-s integration time per pixel, and 6.4- to 7.2-μW excitation power). (**B**) Excitation-resolved APD-based intensity images (20-ms integration time per pixel and 0.5- to 0.6-μW excitation power) of the same region.

taggant loading does not require the digitization to include colocalization, then only combinations involving the pure RGB colors will be present in the images even when the digitization software allow for colocalization.

The exponential law dictates that the encoding capacity quickly rises toward infinity as a function of the number of pixels with both four and seven responses. Because our method grants full control over the size of the imaged area, only data storage and the computing power needed to perform the point-by-point comparison of two digital keys limit the maximum encoding capacity. The actual encoding capacity is determined by the full system. As an example, we use the RGB-CMYK approach with seven responses and an RGB+K approach with four responses and 60 pixels × 60 pixels images resulting in maximum encoding capacities of $7^{3600}$ and $4^{3600}$, respectively. Primarily due to the physical dimensions of the taggants, the actual encoding capacity is reduced to $6 \times 10^{104}$ and $2.1 \times 10^{91}$ (see the Supplementary Materials). If higher encoding capacities are required, then these can be achieved by imaging larger areas or by matching the physical dimensions of the taggants to the pixel size used. By optimizing the full system, the number of responses becomes less important. For example, using only europium and terbium with taggants matched to the pixel size of a video graphics array (VGA) image sensor will result in an actual encoding capacity of $4^{307200}$.

To form the digital key from the raw readout, we used a process involving several steps (see Fig. 5). Several sets of parameters are used in the digitization process. These add another layer of security to the authentication system, because authentication can only be achieved by using the correct parameters. If one parameter is changed, then a different digital key is produced. The input is the three raw images of total emission intensity versus pixel recorded following excitation at one of the three selected wavelengths. Each data set is individually noise-reduced using a relative and an absolute threshold value resulting in three noise-reduced images (Fig. 5A). Below the thresholds, the intensity of pixels is forced to be zero: The relative threshold sets all the pixels of an image that are below a certain percent of the maximum intensity of the image to zero, and the absolute threshold sets all the pixels with less than a certain number of counts per second to zero. The latter avoids considering noise as signal if the image has a poor signal-to-noise ratio. The noise reduction reduces the encoding capacity but is crucial for a proper digitization (see the Supplementary Materials).

In the next step of the process, the three noise-reduced image sets are considered together in a digitization process that results in three binary images (Fig. 5B). The color condition [RGB] of a given pixel depends on the intensity determined in the pixel in all three noise-reduced images and is locked to a hardware-specific level of cross-talk between the laser lines. The cross-talk limits are unique for a given system and add another layer of protection. In the authentication system demonstrated here, we require that the corresponding signal in the $Tb^{3+}$ channel (G) AND/OR $Dy^{3+}$ channel (B) is less than 0.1 times the intensity of the $Eu^{3+}$ channel (R) for a pixel to be [1**]. Otherwise, the pixel is considered [0**]. If we require both conditions to be true (AND operator), then we are using the RGB+K approach, whereas the OR operator allows for colocalization, and is used in the RGB-CMYK approach. By merging the three digitized images, the digital key (Fig. 5C) is created. Note that pixels with colocalization appear black in the RGB+K approach. The file sizes of the corresponding digital keys in either scheme are only 21.09 kilobytes, and the size of the digital file depends only on the number of pixels in the data set (see the Supplementary Materials).

## Authentication

The full authentication system is outlined in Fig. 6. To realize the example in Fig. 6, we suggest that the taggants are included in the polymer used for the blister pack; thus, the physical key is simply a selected area of the pack. The full authentication system contains three levels of security: the physical key, the digitization software including noise reduction and cross-talk definitions, and the acceptance criteria for comparing two digital keys from the same physical key. The acceptance criteria will depend strongly on the reader hardware. When using our setup and the RGB+K scheme, we suggest an acceptance criterion, where an error margin of 40% in each channel is tolerated. This gives rise to a false-positive probability of $3.6 \times 10^{-96}$, which is acceptable for all practical purposes (see the Supplementary Materials). The error margin allows small differences between the individual readers used at separate points in the supply chain. Because the read time is short and digital processing is fast, the false positives can be fully eliminated

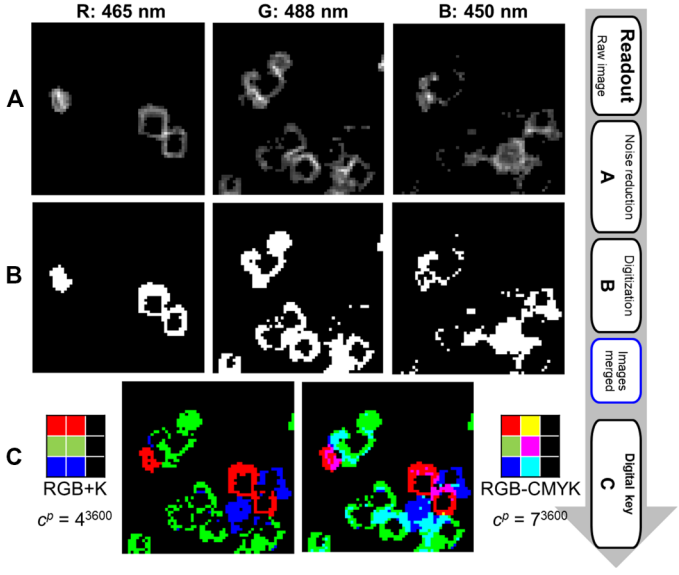


**Fig. 5. Converting the read physical key into a digital key using either four or seven responses.** The digitization process of excitation-selected (R, 465; G, 488; and B, 450 nm) images of one physical key made from a mixture of $Eu^{3+}$-, $Tb^{3+}$-, and $Dy^{3+}$-doped zeolites in PVA (30 μm × 30 μm, 60 pixels × 60 pixels, and 20-ms integration time). (**A**) Noise-reduced images. (**B**) Digitized images in the RGB-CMYK scheme. (**C**) The digital key formed using the RGB+K scheme without co-localization and the RGB-CMYK scheme with colocalization. In the digital key, the colors correspond to $Eu^{3+}$ (R = [100]), $Tb^{3+}$ (G = [010]), $Dy^{3+}$ (B = [001]), $Tb^{3+}$ and $Dy^{3+}$ (C = [011]), $Eu^{3+}$ + $Tb^{3+}$ (Y = [110]), $Eu^{3+}$ + $Dy^{3+}$ (M = [101]), and empty (K = [000]).

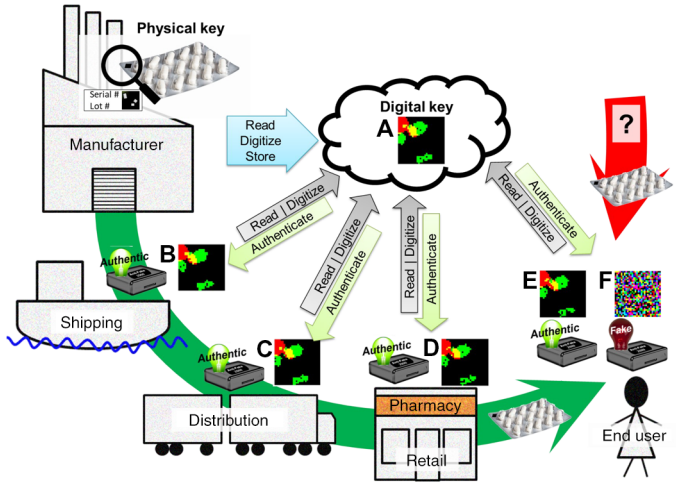


**Fig. 6. An optical authentication system based on imaging of excitation-selected lanthanide luminescence used as an anticounterfeiting system.** A product is authenticated using a physical key and readers at critical points in the supply chain. The physical key is read, digitized (second to fourth read) (**B** to **D**), and matched to the digital key (first read) (**A**) that was stored in the cloud by the manufacturer. Counterfeit products can enter at all points in the supply chain but will be eliminated by trusted retailers (green arrow). Counterfeits may be introduced directly to the end user (red arrow), who then must authenticate the product using a personal reader [fifth read (**E**) or random pattern (**F**)] or consult a trusted retailer.

by performing the authentication operation in triplicate. Note that the acceptance criteria must be tailored to the actual anticounterfeiting tags and hardware used. To demonstrate the authentication system as an anticounterfeiting measure, we have implemented and tested one set of two acceptance criteria. Figure 6 summarizes the requirements of an anticounterfeiting system, where products must be authenticated at all points in the supply chain (*41*, *42*), and includes an example where we have challenged our system with two products with an authentic and a fake anticounterfeiting tag. The PUF tag was registered at the point of origin by reading the physical key and storing a copy of the digital key. The digital key was then used to authenticate the physical key, which was reread four times to illustrate the different points in the supply chain. Physical keys that did not match the digital key were not authenticated (see the Supplementary Materials).

In summary, we have demonstrated an optical authentication system, exploiting the unique optical properties of trivalent lanthanide ions, PUFs, state-of-the-art optical technology, and cryptographic approaches. The optical authentication system can be used for unbreakable encryption but was demonstrated for anticounterfeiting purposes. When used as an anticounterfeiting system, the manufacturer tags a product with a unique physical key and records the digital key corresponding to the PUF key in a read-only public database. The number of unique physical keys is near infinite, and coincidentally identical anticounterfeiting tags will not occur. In addition, because the PUF key is unique and cannot be copied, there is no need for secrecy. Merchants and end users can then verify the authenticity of the product using shop-based or personal readers that, knowing the type of product, look up the digital key in the corresponding manufacturers' section of the database. The large parameter space of the randomly generated PUF keys made from affordable materials enables a simple approach to authentication of consumer goods, medicine, passports, or electronic components subjected to counterfeiting. The robust physical keys can either be grafted onto the product or supplied as thin films. The fundamental properties of the lanthanide ions exploited in excitation-selected imaging cannot be emulated, the structures cannot be printed, and product keys are registered by trusted manufacturers. All three facts would individually make the method tamper-proof. The economic benefit in upholding trademark and intellectual property rights is substantial, and using the excitation-selected imaging of lanthanide-doped zeolites to ensure the authenticity of medicine will save lives.

## MATERIALS AND METHODS

Tb(III) acetate hydrate (99.9%) and Eu(III) acetate hydrate (99.9%) were purchased from Sigma-Aldrich, and Dy(III) acetate hydrate (99.9%) was purchased from Strem Chemicals. LTA zeolites were a gift from UOP Antwerpen PVA (98% hydrolyzed; average $M_w$, 13,000 to 23,000) was purchased from Sigma-Aldrich. All chemicals were used as received. Milli-Q water was used to prepare all reagents.

### Loading of zeolites with lanthanides

To exchange the $Ca^{2+}$ cations within the pores and cavities of the LTA zeolite with $Ln^{3+}$ cations ($Dy^{3+}$, $Eu^{3+}$, or $Tb^{3+}$), 200 mg of LTA was mixed with 800 μl of 0.25 M $Ln^{3+}$ acetate hydrate dissolved in Milli-Q water and mixed overnight (IKA Vortex 3) at room temperature. The $Ln^{3+}$-exchanged zeolites were recovered and washed three times with 1 ml of Milli-Q water by centrifugation (1000 rpm, 2 min; Force 12, Denver Instrument) and then dispersed into 1 ml of Milli-Q water. For the model system validation, 1 mg of each $Ln^{3+}$-doped zeolites in 3% (w/v) PVA/water was spin-coated on a 22-mm × 22-mm microscope glass slide (Menzel-Gläser no. 1.5) for ~1 min to form a thin film.

### $Ln^{3+}$ spectroscopy

Absorption spectra (Lambda 1050 UV/Vis/NIR spectrometer, PerkinElmer) and fluorescence excitation spectra (Cary Eclipse Fluorescence Spectrophotometer, Agilent Technologies) were measured from 0.1 to 0.2 M $Ln^{3+}$ acetate hydrate solutions in 2-ml Milli-Q water from a quartz cuvette with a path length of 10 mm (Starna Scientific). Absorption spectra were recorded using a double-beam setup with Milli-Q water in the reference channel and corrected for baseline and dark current. A $Ho^{3+}$ oxide standard was used for wavelength calibration. Excitation spectra were recorded with 2.5-nm excitation slits, 5-nm emission slits, and 1000 V on the detector.

### Hardware setup

The confocal microscopy setup depicted in fig. S1 was used for the excitation-selected imaging. A SuperK EXTREME EXB-6 supercontinuum white light laser with a SuperK SELECT wavelength selector (NKT Photonics) was used as the excitation source. Three excitation wavelengths were selected: 465, 488, and 450 nm. For spectral imaging, the laser powers with 77.88-MHz repetition rate for each wavelength were 6.4, 6.9, and 7.2 μW. For total intensity imaging, the laser powers 25.96-MHz repetition rate were 0.5, 0.6, and 0.6 μW, that is, one-twelfth of the powers used in spectral imaging. Short-pass filters [SP1 (FES0500, Thorlabs) and SP2 (540AESP, Omega Optical)] were added to the excitation light path.

The homebuilt scanning fluorescence confocal microscopy setup was based on an Olympus IX71 inverted microscope with a piezo-driven scanning stage (P5173CL, Physik Instrumente), controlled by a home-written software program (LabVIEW, National Instruments), allowing for point-by-point imaging of the sample in a raster scanning fashion in a range of up to 100 μm × 100 μm. Upon laser illumination, the emission signal from the sample was collected by the same 100× oil immersion objective (Olympus UPLFLN; numerical aperture, 1.3). A 70/30 beam splitter (XF122, Omega Filters) was used in the microscope instead of a dichroic mirror. A 50-μm pinhole was used in the detection path.

For the spectral imaging, the emission light was directed through optical filters [LP (2× BLP01-532R-25) and SP3 (SP01-633RS-25); both from Semrock] and into a nitrogen-cooled CCD-based spectrometer [Princeton Instruments SPEC-10:100B/LN_eXcelon CCD camera and SP-2356 spectrometer with 1-030-500 grating (300 grooves/mm at 500 nm); all controlled by the same LabVIEW program that controls the scanner]. The *x* axis of the emission spectra was calibrated using emission lines of a neon lamp (6032 neon lamp, Newport Corporation). The *y* axis (intensity) was not corrected for differences in optical transmission and detection efficiency.

For the total intensity–based imaging, the emission light was directed through the same optical filters (LP and SP3) and into an APD (CD3226, PerkinElmer) connected to time-correlated single photon counting electronics (SPC-830, Becker & Hickl). A home-written MATLAB (MathWorks) routine was used to create images from the recorded first in, first out (FIFO) data files [see the Supplementary information in the study of Liao *et al.* (*40*)]. The optimized filters SP1, SP2, LP, and SP3 were always used in the data described in the section "Excitation-selected imaging" and onward in the Supplementary Materials. The full spectral information was recorded without SP3 when investigating the model system.

## SUPPLEMENTARY MATERIALS

Supplementary material for this article is available at http://advances.sciencemag.org/cgi/content/full/4/1/e1701384/DC1



## REFERENCES AND NOTES

1. R. R. Gosline, *Forbes*, 12 February 2010; http://forbes.com/2010/02/11/luxury-goods-counterfeit-fakes-chanel-gucci-cmo-network-renee-richardson-gosline.html.
2. J. Rogin, *The Daily Beast*, 12 February 2014; http://thedailybeast.com/articles/2014/02/12/the-u-s-tells-you-where-to-buy-the-best-fake-designer-handbags-pirated-movies-and-more.html.
3. Organization for Economic Cooperation and Development (OECD)/European Union Intellectual Property Office, *Trade in counterfeit and pirated goods: Mapping the economic impact* (OECD Publishing, 2016).

4. U.S. Food and Drug Administration, *Counterfeit Medicine* (U.S. Department of Health and Human Services, 2016); http://fda.gov/Drugs/ResourcesForYou/Consumers/BuyingUsingMedicineSafely/CounterfeitMedicine/default.htm.
5. T. K. Mackey, B. A. Liang, The global counterfeit drug trade: Patient safety and public health risks. *J. Pharm. Sci.* **100**, 4571–4579 (2011).
6. P. N. Newton, M. D. Green, F. M. Fernández, N. P. J. Day, N. J. White, Counterfeit anti-infective drugs. *Lancet Infect. Dis.* **6**, 602–613 (2006).
7. P. Aldhous, Counterfeit pharmaceuticals: Murder by medicine. *Nature* **434**, 132–136 (2005).
8. C. Sheridan, Bad medicine. *Nat. Biotechnol.* **25**, 707–709 (2007).
9. R. Horstmeyer, B. Judkewitz, I. M. Vellekoop, S. Assawaworrarit, C. Yang, Physical key-protected one-time pad. *Sci. Rep.* **3**, 3543 (2013).
10. M. Lehtonen, N. Oertel, H. Vogt, in *2007 IEEE International Technology Management Conference (ICE)* (IEEE, 2007), pp. 1–8.
11. E. L. Prime, D. H. Solomon, Australia's plastic banknotes: Fighting counterfeit currency. *Angew. Chem. Int. Ed.* **49**, 3726–3736 (2010).
12. J. Gooch, B. Daniel, V. Abbate, N. Frascione, Taggant materials in forensic science: A review. *TrAC Trends Anal. Chem.* **83** Part B, 49–54 (2016).
13. H. J. Bae, S. Bae, C. Park, S. Han, J. Kim, L. N. Kim, K. Kim, S. H. Song, W. Park, S. Kwon, Biomimetic microfingerprints for anti-counterfeiting strategies. *Adv. Mater.* **27**, 2083–2089 (2015).
14. R. Pappu, B. Recht, J. Taylor, N. Gershenfeld, Physical one-way functions. *Science* **297**, 2026–2030 (2002).
15. A. F. Smith, P. Patton, S. E. Skrabalak, Plasmonic nanoparticles as a physically unclonable function for responsive anti-counterfeit nanofingerprints. *Adv. Funct. Mater.* **26**, 1315–1321 (2016).
16. R. Arppe, T. J. Sørensen, Physical unclonable functions generated through chemical methods for anti-counterfeiting. *Nat. Rev. Chem.* **1**, 0031 (2017).
17. Y. Geng, J. H. Noh, I. Drevensek-Olenik, R. Rupp, G. Lenzini, J. P. F. Lagerwall, High-fidelity spherical cholesteric liquid crystal Bragg reflectors generating unclonable patterns for secure authentication. *Sci. Rep.* **6**, 26840 (2016).
18. Z. Hu, J. M. M. Lobez Comeras, H. Park, J. Tang, A. Afzali, G. S. Tulevski, J. B. Hannon, M. Liehr, S.-J. Han, Physically unclonable cryptographic primitives using self-assembled carbon nanotubes. *Nat. Nanotechnol.* **11**, 559–565 (2016).
19. J. Kim, J. M. Yun, J. Jung, H. Song, J.-B. Kim, H. Ihee, Anti-counterfeit nanoscale fingerprints based on randomly distributed nanowires. *Nanotechnology* **25**, 155303 (2014).
20. L. Tian, K.-K. Liu, M. Fei, S. Tadepalli, S. Cao, J. A. Geldmeier, V. V. Tsukruk, S. Singamaneni, Plasmonic nanogels for unclonable optical tagging. *ACS Appl. Mater. Interfaces* **8**, 4031–4041 (2016).
21. T. A. W. Wolterink, R. Uppu, G. Ctistis, W. L. Vos, K.-J. Boller, P. W. H. Pinkse, Programmable two-photon quantum interference in $10^3$ channels in opaque scattering media. *Phys. Rev. A* **93**, 053817 (2016).
22. J. D. R. Buchanan, R. P. Cowburn, A.-V. Jausovec, D. Petit, P. Seem, G. Xiong, D. Atkinson, K. Fenton, D. A. Allwood, M. T. Bryan, Forgery: 'Fingerprinting' documents and packaging. *Nature* **436**, 475 (2005).
23. C. Herder, M.-D. Yu, F. Koushanfar, S. Devadas, Physical unclonable functions and applications: A tutorial. *Proc. IEEE* **102**, 1126–1141 (2014).
24. Y. Zheng, C. Jiang, S. H. Ng, Y. Lu, F. Han, U. Bach, J. J. Gooding, Unclonable plasmonic security labels achieved by shadow-mask-lithography-assisted self-assembly. *Adv. Mater.* **28**, 2330–2336 (2016).
25. M. Wang, B. Duong, H. Fenniri, M. Su, Nanomaterial-based barcodes. *Nanoscale* **7**, 11240–11247 (2015).
26. J. M. Meruga, W. M. Cross, P. S. May, Q. Luu, G. A. Crawford, J. J. Kellar, Security printing of covert quick response codes using upconverting nanoparticle inks. *Nanotechnology* **23**, 395201 (2012).
27. Y. Lu, J. Zhao, R. Zhang, Y. Liu, D. Liu, E. M. Goldys, X. Yang, P. Xi, A. Sunna, J. Lu, Y. Shi, R. C. Leif, Y. Huo, J. Shen, J. A. Piper, J. P. Robinson, D. Jin, Tunable lifetime multiplexing using luminescent nanocrystals. *Nat. Photonics* **8**, 32–36 (2014).
28. D. J. Chandler, B. A. Lambert, J. J. Reber, S. L. Phipps, "Precision fluorescently dyed particles and methods of making and using same," U.S. Patent 6,514,295 (2003).
29. S. Fournier-Bidoz, T. L. Jennings, J. M. Klostranec, W. Fung, A. Rhee, D. Li, W. C. W. Chan, Facile and rapid one-step mass preparation of quantum-dot barcodes. *Angew. Chem. Int. Ed.* **47**, 5577–5581 (2008).
30. X.-H. Ji, N.-G. Zhang, W. Cheng, F. Guo, W. Liu, S.-S. Guo, Z.-K. He, X.-Z. Zhao, Integrated parallel microfluidic device for simultaneous preparation of multiplex optical-encoded microbeads with distinct quantum dot barcodes. *J. Mater. Chem.* **21**, 13380–13387 (2011).
31. Q. Wang, Y. Liu, C. Lin, H. Yan, Layer-by-layer growth of superparamagnetic, fluorescent barcode nanospheres. *Nanotechnology* **18**, 405604 (2007).
32. M. Han, X. Gao, J. Z. Su, S. Nie, Quantum-dot-tagged microbeads for multiplexed optical coding of biomolecules. *Nat. Biotechnol.* **19**, 631–635 (2001).
33. J.-C. G. Bünzli, S. V. Eliseeva, in *Lanthanide Luminescence: Photophysical, Analytical and Biological Aspects*, P. Hänninen, H. Härmä, Eds. (Springer-Verlag, 2010), vol. 7, pp. 1–46.
34. K. A. White, D. A. Chengelis, K. A. Gogick, J. Stehman, N. L. Rosi, S. Petoud, Near-infrared luminescent lanthanide MOF barcodes. *J. Am. Chem. Soc.* **131**, 18069–18071 (2009).
35. M. J. Dejneka, A. Streltsov, S. Pal, A. G. Frutos, C. L. Powell, K. Yost, P. K. Yuen, U. Müller, J. Lahiri, Rare earth-doped glass microbarcodes. *Proc. Natl. Acad. Sci. U.S.A.* **100**, 389–393 (2003).
36. J. Andres, R. D. Hersch, J.-E. Moser, A.-S. Chauvin, A new anti-counterfeiting feature relying on invisible luminescent full color images printed with lanthanide-based inks. *Adv. Funct. Mater.* **24**, 5029–5036 (2014).
37. J. Lee, P. W. Bisso, R. L. Srinivas, J. J. Kim, A. J. Swiston, P. S. Doyle, Universal process-inert encoding architecture for polymer microparticles. *Nat. Mater.* **13**, 524–529 (2014).
38. M. Alvaro, V. Fornés, S. García, H. García, J. C. Scaiano, Intrazeolite photochemistry. 20. Characterization of highly luminescent europium complexes inside zeolites. *J. Phys. Chem. B* **102**, 8744–8750 (1998).
39. Z. Liao, M. Tropiano, K. Mantulnikovs, S. Faulkner, T. Vosch, T. J. Sørensen, Spectrally resolved confocal microscopy using lanthanide centred near-IR emission. *Chem. Commun.* **51**, 2372–2375 (2015).
40. Z. Liao, M. Tropiano, S. Faulkner, T. Vosch, T. J. Sørensen, Time-resolved confocal microscopy using lanthanide centred near-IR emission. *RSC Adv.* 70282–70286 (2015).
41. M. Lehtonen, in *Unique Radio Innovation for the 21st Century: Building Scalable and Global RFID Networks*, C. D. Ranasinghe, Z. Q. Sheng, S. Zeadally, Eds. (Springer-Verlag, 2011), pp. 331–351.
42. L. Li, Technology designed to combat fakes in the global supply chain. *Bus. Horiz.* **56**, 167–177 (2013).


**Acknowledgments:** We thank UOP Antwerpen for donating the LTA zeolites.
**Funding:** This work was supported by the Villum Fonden (grant no. 14922), Villum Fonden block stipends, bioSYNergy University of Copenhagen's Excellence Programme for Interdisciplinary Research, the "Center for Synthetic Biology" at Copenhagen University funded by the UNIK research initiative of the Danish Ministry of Higher Education and Science (grant no. 09-065274), and the Danish Council of Independent Research (grant no. DFF-1323-00352). **Author contributions:** M.R.C.-T. and R.A. manufactured the PUF-tags and performed the experiments and the initial data analysis. M.R.C.-T. wrote the software and did the mathematical modeling. R.A. and T.J.S. wrote the first draft of the paper. T.V. and T.J.S. came up with the idea and supervised the experiments. All authors contributed to the final version of the manuscript. **Competing interests:** All authors of this paper are inventors of a patent application related to this work that has been filed with the European Patent Office by the University of Copenhagen (application no. EP17152670.0, filed 23 January 2017). **Data and materials availability:** All data needed to evaluate the conclusions in the paper are present in the paper and/or the Supplementary Materials. Additional data related to this paper may be requested from the authors.

Submitted 10 May 2017
Accepted 15 December 2017
Published 26 January 2018
10.1126/sciadv.1701384

**Citation:** M. R. Carro-Temboury, R. Arppe, T. Vosch, T. J. Sørensen, An optical authentication system based on imaging of excitation-selected lanthanide luminescence. *Sci. Adv.* **4**, e1701384 (2018).

# An optical authentication system based on imaging of excitation-selected lanthanide luminescence

Miguel R. Carro-Temboury, Riikka Arppe, Tom Vosch and Thomas Just Sørensen

*Sci Adv* **4** (1), e1701384.
DOI: 10.1126/sciadv.1701384